HHS Public Access

Author manuscript

Ann Neurol. Author manuscript; available in PMC 2019 April 01.

Published in final edited form as:

Ann Neurol. 2018 April ; 83(4): 756–770. doi:10.1002/ana.25198.

Myelin Abnormality in CMT4J Recapitulates Features of Acquired Demyelination

Bo Hu, MD,PhD[1], **Megan Mccollum, MS**[1], **Vignesh Ravi**[1], **Sezgi Arpag, MS**[1], **Daniel Moiseev**[1], **Ryan Castoro, MD,PhD**[2], **Bret C. Mobley, MD**[3], **Bryan W. Burnette, MD**[4], **Carly Siskind, MS**[5], **John W. Day, MD,PhD**[5], **Robin Yawn, MS**[1], **Shawna Feely, MS**[6], **Yuebing Li, MD,PhD**[7], **Qing Yan, MS**[1,8], **Michael E. Shy, MD**[6], and **Jun Li, MD,PhD**[1,9]

[1]Department of Neurology, Center for Human Genetic Research, and Vanderbilt Brain Institute, Vanderbilt University Medical Center, Nashville, Tennessee

[2]Department of PMR, Vanderbilt University Medical Center, Nashville, Tennessee

[3]Department of Pathology, Vanderbilt University Medical Center, Nashville, Tennessee

[4]Department of Pediatrics, Vanderbilt University Medical Center, Nashville, Tennessee

[5]Department of Neurology, Stanford University, Palo Alto, California

[6]Department of Neurology, University of Iowa, Iowa City, Iowa

[7]Department of Neurology, Cleveland Clinic Foundation, Cleveland, Ohio

[8]Department of Laboratory Medicine, the Second Affiliated Hospital of Qingdao University, Qingdao, China

[9]Tennessee Valley Healthcare System – Nashville VA, Nashville, Tennessee

Abstract

Objective—Charcot-Marie-Tooth type 4J (CMT4J) is a rare autosomal recessive neuropathy caused by mutations in *FIG4* that result in loss of FIG4 protein. This study investigates the natural history and mechanisms of segmental demyelination in CMT4J.

Methods—Over the past 9 years, we have enrolled and studied a cohort of 12 CMT4J patients, including 6 novel *FIG4* mutations. We evaluated these patients and related mouse models using morphological, electrophysiological and biochemical approaches.

Results—We found sensory motor demyelinating polyneuropathy consistently in all patients. This underlying myelin pathology was associated with non-uniform slowing of conduction velocities, conduction block, and temporal dispersion on nerve conduction studies (NCS), which resemble those features in acquired demyelinating peripheral nerve diseases. Segmental

Corresponding author: Jun Li, MD, PhD; Department of Neurology, Vanderbilt University School of Medicine, 1161 21th Avenue South, Nashville, TN 37232. jun.li.2@vanderbilt.edu.

Author contributions:
B.H., M.S., V.R., S.A.; D.M.; R.C.; B.B.; C.S.; J.D.; R.Y.; S.F.; Y.B.L; Q.Y.; M.S. and J.L. contributed to data acquisition and analysis. J.L. contributed to study concept, design and manuscript preparation.

Potential Conflicts of Interest:
Nothing to report.

demyelination was also confirmed in mice without *Fig4* (*Fig4*$^{-/-}$). The demyelination was associated with an increase of Schwann cell dedifferentiation and macrophages in spinal roots where nerve blood barriers are weak. Schwann cell dedifferentiation was induced by the increasing intracellular Ca^{2+}. Suppression of Ca^{2+} level by a chelator reduced dedifferentiation and demyelination of Schwann cells *in vitro* and *in vivo*. Interestingly, cell-specific knockout of *Fig4* in mouse Schwann cells or neurons failed to cause segmental demyelination.

Interpretation—Myelin change in CMT4J recapitulates the features of acquired demyelinating neuropathies. This pathology is not Schwann cell autonomous. Instead, it relates to systemic processes involving interactions of multiple cell types and abnormally elevated intracellular Ca^{2+}. Injection of a Ca^{2+} chelator in *Fig4*$^{-/-}$ mice improved segmental demyelination, thereby providing a therapeutic strategy against demyelination.

Keywords

Charcot-Marie-Tooth disease; CMT4J; FIG4; I41T; segmental demyelination; dysmyelination; inherited neuropathy; neuronal degeneration; lysosomalfission; lysosomal storage; nerve conduction study; EMG; amyotrophic lateral sclerosis

Introduction

Myelinated axons are wrapped by Schwann cell membranes (myelin) in segments (internodes). The segments are separated by punctate gaps, called nodes of Ranvier, where the axon is denuded of myelin. This configuration facilitates the saltatory conduction of action potentials.

Peripheral neuropathies resulting from genetic mutations often affect myelination during development, called **dys**myelination, as seen in Charcot-Marie-Tooth type-1A (CMT1A) caused by *PMP22* duplication. CMT1A dysmyelination[1] causes shortened internodes and *uniform* slowing of conduction velocity (CV), which denotes slowed CV with minimal variations between different nerves in an affected patient[2]. In contrast, the slowing of CV in patients with acquired demyelinating diseases is *non-uniform* and often coexistent with temporal dispersion and/or conduction block. Pathologically, nerve fibers demonstrate removal of myelin in a portion of internodes and normal myelin in other internodes, called segmental **de**myelination[3].

Demyelination is the primary pathology in a long list of neurological disorders, including chronic inflammatory demyelinating polyneuropathy (CIDP) and Guillain-Barré Syndrome. Despite the increasing treatment options (predominantly immunomodulatory), disabilities still develop in patients with demyelinating diseases. This is largely due to a general lack of understanding of the molecular mechanisms that regulate demyelination.

FIG4 is a phosphatase with specificity toward the 5'-phosphate in phosphatidylinositol-3,5-disphosphate ($PI3,5P_2$), which plays an important role in regulating lysosomal membrane trafficking. While FIG4 can decrease $PI3,5P_2$ levels via its phosphatase action, it can also promote $PI3,5P_2$ synthesis by acting as a secondary scaffold. FIG4 (**S**AC3) complexes with Vac14 (=**A**rPIKfyve in mammalian cells) which then interacts with and activates the 5'-

kinase of PI3P known as Fab1 (=**P**IKfyve)[4,5]. This **PAS** complex mediates the conversion of PI3P to $PI3,5P_2$[6,7]. Promotion of $PI3,5P_2$ synthesis is the dominant function of FIG4 since loss of FIG4 results in a reduction of $PI3,5P_2$[8,9]. $PI3,5P_2$ has been critically involved in endolysosomal trafficking. Indeed, ablation of *Fig4* in pale tremor (*plt = Fig4*$^{-/-}$) mice decreases $PI3,5P_2$ level[8] and produces excessive lysosomal storage[9].

TRPML-1, a Ca^{2+}-channel on lysosomal membranes, is specifically gated by $PI3,5P_2$ to release Ca^{2+} from lysosomes[10]. Therefore, $PI3,5P_2$ deficiency in *Fig4*$^{-/-}$ cells would deactivate the TRPML-1 channel and impair lysosomal membrane trafficking. Indeed, our studies have shown increased intralysosomal Ca^{2+} and impaired lysosomal fission in *Fig4*$^{-/-}$ cells, including myelinating Schwann cells[11]. Lysosomal membrane trafficking has been suggested to be important for myelination[12,13].

In this study, we studied 12 patients with CMT4J enrolled over the past 9 years, as well as relevant mouse models. Unlike certain subtypes of CMT1 with uniform slowing of CV, non-uniform slowing with temporal dispersion and conduction block was found in patients with CMT4J. Similar nerve conduction changes were observed in FIG4 deficient mice correlating with removal of internodal myelin and macrophage increase in spinal roots. These features recapitulate those seen in acquired demyelinating diseases, indicating that understanding FIG4 deficiency may reveal novel molecular pathways that alter lysosomal functions common to both genetic and acquired forms of demyelination.

Subjects and Methods

Patients

Twelve patients have been prospectively evaluated (by J.L. or M.E.S.) at Vanderbilt Medical Center or University of Iowa. Note that case #2, 9 and 10 were published before[14,15]. New data on these three cases were included here. This study was approved by the Institutional Review Board (IRB) in both institutions. A written consent / assent were obtained from all participants.

CMT neuropathy score (CMTESv2)[16] was obtained for most patients (listed in Table 1). CMTES ranges from 0 to 28, with higher scores indicating increased disease severity.

Nerve Conduction Studies (NCS)

NCS data in humans were acquired using conventional methods[17]. Conduction block was defined as 50% reduction of compound muscle action potential (CMAP) evoked by proximal stimulation[18]. Temporal dispersion was defined as dis-synchronized CMAP with two or more extra phases and 30% increase of negative peak duration. Mouse NCS were described previously[19].

DNA Sequencing

Patient DNA was evaluated by targeted gene-panel next-generation sequencing, a service provided by Medical Neurogenetics (Atlanta, GA), GeneDx (Gaithersburg, MD), Invitae (San Francisco, CA) or Athena Diagnostics (Worcester, MA). Specific mutations in *FIG4* were verified by Sanger sequencing.

Primary human fibroblast culture and lysosomal fission assay

Primary human fibroblast culture was described previously[20]. Lysosomal fission was tested as described previously[11]. Fibroblasts in culture were treated with vehicle or vacuolin-1 (5μM, Cat# 673000, Sigma) for 1.5 hours to increase lysosome size and cells were imaged. After removal of vacuolin-1, cells were allowed to recover their lysosomal sizes through fission. At the end of the 8th hour after washing out, cells were imaged again. Percentages of cells with vacuoles ≥3μM in diameters were counted.

RNA extraction and RT-PCR for exon skipping analysis

Total RNA was isolated from the fibroblasts using Trizol reagents. Reverse transcription was performed in 1μg RNA using random hexamer primer mixture (Cat# 04379012001, Roche). *FIG4* cDNA was amplified using primers: for the 451bp product, forward, 5'-GGACACCAGAGGTGATAAAG-3' and reverse, 5'- CCTGCATCAGTCATCTTCAC - 3'; for the 612bp product, forward, 5'- GCCTAAGACCGTTGGAATTG - 3' and reverse, 5'-TAGCGGTTCCTGATGTACTC - 3'. PCR reactions were performed in 1μl of cDNA. PCR was performed for 40 cycles (denaturation at 95°C for 1 minute, annealing at 57°C for 30 seconds and extension at 72°C for 1 minute). The PCR products were separated on 2% agarose gel. The sequence around exons 18 and 22 was determined by Sanger sequencing.

Western blot

Proteins from fibroblasts were extracted using RIPA buffer with proteinase/phosphatase inhibiter cocktail (Cat# 5872, Cell Signaling). Samples were loaded into SDS-PAGE gels, transferred to PVDF membrane and blotted with primary antibodies, followed by secondary antibodies. The immune complexes were detected by the chemoilluminescence.

Animal models

Pale tremor (*plt = Fig4*$^{-/-}$) mouse from Jackson was a spontaneously occurring mutant following insertion of a *Fig4* disrupting transposon which blocked its expression[8]. This mouse was backcrossed with C57B6 over nine generations to reach congenic background.

Design and production of *Fig4*$^{flox/flox}$ (=*Fig4*$^{f/f}$) mouse are detailed in Figure 7 below. We crossed *Fig4*$^{f/f}$ mice with myelin protein zero – cre (*Mpz*^{cre}) mice (Jackson; stock #017927) to produce Schwann cell specific knockout (*scFig4*$^{-/-}$) mice. We produced the neuron-specific knockouts (*nFig4*$^{-/-}$) by crossing *Fig4*$^{f/f}$ mice with neuron-specific synapsin-cre mice (*Syn*^{Cre}; Jackson, stock #003966). All mice were on the C57B6 background.

Teased nerve fiber preparation, paraffin embedding, and immunofluorescence staining

Teased nerve fiber analysis was described previously[21]. In brief, nerves were fixed in 4% paraformaldehyde for 30 minutes – 16 hours (depending on primary antibodies used). Sciatic nerves were teased into individual fibers on glass-slides. Slides were dried overnight, reacted with primary antibodies and then incubated for 1.5 hours with secondary antibodies. Slides were examined under a Leica fluorescent microscope (Leica DM6000B). Paraffin sections were prepared according to previously published methods[22]. They were stained with a similar procedure above.

Antibodies

The following antibodies were from Cell Signaling: c-Jun (Cat# 9165), Notch-1(Cat# 3608), Phospho-c-Jun (Cat# 2361), Sox2 (Cat# 4900), Phospho-JNK (Cat# 4668), JNK (Cat# 9252), Phospho-Erk1/2 (Cat# 4370), Erk1/2 (Cat# 4695) and β-Tubulin (Cat# 2128). Abcam: Sox10 (Cat# ab27655), Egr2 (Cat# ab43020), -actin (Cat# ab8227) and GAPDH (Cat# ab9485). Bio-Rad: CD68 (Cat# MCA1957). Neuromab: Fig4 (Cat# 75-201). Millipore: P75 (Cat# ab1554).

Semithin section and internodal length quantification

These techniques have been described previously[14]. The semithin sections were stained with toluidine blue and examined by light microscopy. The 9-mm nerve segment in liquid Epon was teased into individual nerve fibers for imaging. The internodal length was measured by software (Leica 6000B).

Morphometric analysis

Five images were captured across the entire area of each sciatic nerve transverse section under 100× lens through a Leica microscope. AxonSeg, an open source Matlab tool (Institute of Biomedical Engineering, Polytechnique Montrea)[23], was used to automatically label the myelin on the images, producing a mask image with minimal manual intervention. ImageJ (1.51n) was used to split the resulting mask image into two: one for inner ellipses of the myelin sheath and the other for outer. ImageJ's built-in "measure particles" command was used to measure the area of each ellipse and its position on the image. Axon density, myelin thickness and g-ratio were calculated from these measurements.

Statistics

For comparison of internodal length between wild-type and *Fig4*$^{-/-}$ mice, a linear mixed effect model was used for outcome Internodal Length, fixed effect Group (*wt vs Fig4*$^{-/-}$) and random *Animal* effects. The random effects were included to account for correlations between lengths on the same animal. Because both fixed and random effects were included, this model was a mixed effects model. To compare CV or CMAP in different groups (e.g. *wt* vs. *Fig4*$^{-/-}$), a non-parametric Wilcoxon Rank-Sum test was used.

Results

Natural history in patients with CMT4J demonstrates sensory motor demyelinating polyneuropathy that recapitulates features in acquired demyelinating diseases

Clinical phenotypes—Phenotypic details are listed in Table 1A. The 12 patients were separable into three groups based on their ages of symptom onset: early onset (n = 3) with severe limb paralysis at birth, teenage onset with mild to severe limb weakness upon their 1st visit (n = 7) and adult onset (n = 2) with mild weakness in their 1st visit. Onset was defined as the age at which medical attention was first sought for a related major neurological symptom. This definition disregarded subtle complaints such as fatigue, mild foot deformities, occasional tripping or ankle twisting, which may be present in all patients, but onset was difficult to recall. A case of CMT4J is described below as an example.

Case #1 (teenage onset: This is a 17-year-old boy who met all developmental milestones. His mother noticed his feet slapping on the ground when walking at 12 years of age. He sprained his ankles many times. Over the previous two years, he had started to buckle his knees and fall, which prompted the initial neurological evaluation. He denied any sensory disturbance. He has excelled academically. On neurological examination, he had hammer toes with high-arched feet. His muscle strength was 4 in distal but 5 in proximal muscles of limbs. He had decreased pinprick, touch and vibration sensation in his feet. Deep tendon reflexes were absent.

Rare phenotypes: CNS involvement and/or rapidly progressive irreversible asymmetric weakness—Nine of the 12 patients showed no obvious CNS symptoms. Brain MRI data in two of the nine patients showed no abnormality. Case #4 and #5 in the early onset group developed mental retardation with brain white matter changes visualized on MRI (Table 1; Figure 1A). However, both cases possessed another mutation – trisomy of chromosome 21 in case #4 and glycerol kinase deficiency (exon 19 deletion in *GK* gene on Xp21.2) in case #5. Case #2 in the teenage onset group presented with Parkinson-like symptoms in addition to polyneuropathy (case report by Orengo et al in Annals of Clinical & Translational Neurology 2017, in press). DNA testing for whole chromosomes was not done. Despite CNS symptoms, demyelinating polyneuropathy in NCS was still present in the three cases. Case #5 had a sural nerve biopsy showing thinly myelinated nerve fibers with severe loss of large myelinated axons (Figure 1C–D). Therefore, CNS symptoms are uncommon among patients with CMT4J. In those cases with conspicuous CNS abnormalities, second genetic mutations should be sought.

Minor trauma has been associated with rapidly progressive asymmetric weakness in case #10 (ALS-like phenotype), which was irreversible until her death[14]. Furthermore, genetic studies in two large cohorts of patients with ALS have revealed some *FIG4* variants as genetic risk factors but not causal for the disease[24,25]. In the present cohort, none had the phenotype of rapidly progressive asymmetric weakness, including four patients (case #3, 6, 7, 8) who had a fall or surgeries but did not develop any rapid progression of weakness after trauma. Case #12 developed asymmetric weakness in the left leg, but it was chronic and slowly progressive. Case #6 developed a transient exacerbation of weakness during pregnancy but stabilized after IVIG treatment (Table 1A).

Electrophysiological findings recapitulate features in acquired demyelinating neuropathies—NCS data in Table 1B showed a highly consistent pattern of sensory motor demyelinating polyneuropathy in all cases with several striking features: 1). Unlike CMT1A patients in which there is uniform slowing of CV[3], patients with CMT4J showed non-uniform slowing of CV. For instance, case #3 showed a CV of 29 m/s in the left median nerve and 39 m/s in the left ulnar nerve. Nine cases had conduction block[26]. Conduction block was difficult to be assessed in three pediatric cases since submaximal stimulations may be used in children. Of six cases with CMAP waveforms available for review, three of six showed temporal dispersion (Figure 1B). 2). Because some nerves had CV below 10 m/s, the decreases of CVs were too severe to be a secondary change from axonal loss (Table 1B). These observations support a primary rather than secondary demyelinating process. 3). Of 8

patients who had needle EMG, six showed fibrillations, positive waves and reduced recruitment of motor unit action potentials indicative of axonal degeneration (Table 1B).

Taken together, a consistent phenotype in patients with CMT4J is sensory motor demyelinating polyneuropathy with features recapitulating acquired demyelinating polyneuropathies. This NCS feature is also in line with the pathological findings in sural nerve biopsies shown in Figure 1C and a 60% de-/remyelination in teased nerve fiber preparation previously reported[14].

Mutations in all CMT4J patients resulted in loss-of-function of FIG4

Mutations in all 12 cases (Table 1A) were evaluated by two servers - PolyPhen-2[27] and SIFT[28]. Both PolyPhen-2 and SIFT predicted that all identified *FIG4* mutations were pathogenic. To further substantiate the pathogenicity, we performed Western blot on protein lysates extracted from fibroblasts cultured from all patients' skin biopsies. FIG4 proteins were either absent or severely reduced when blotted by anti-FIG4 antibodies (Figure 2A).

Case #2 and #5 had intronic mutations (Table 1A). We performed PCR on cDNA isolated from their fibroblasts with primers flanking the intronic mutations. In case #2, we identified a shortened band in addition to the normal allelic band (Figure 2B), confirming the previous report[15]. The shortened band was cut and sequenced, which showed a deletion of exon 18 (Figure 2C), thereby demonstrating abnormal splicing due to the intronic mutation. In case #5, a deletion of exon 22 by abnormal splicing was identified (Figure 2D–E).

Interestingly, case #3 with normal strength had a FIG4 protein level that was about four times higher than those in the other 11 patients (Figure 2A). The levels of FIG4 were not significantly different between early and teenage onset groups (0.05±0.02 vs. 0.05±0.03, $p>0.05$; these numbers were relative values over loading control).

Case #12 had homozygous mutations of *I41T*. I41T mutation has been shown to destabilize FIG4 leading to a rapid degradation of FIG4 by proteasomes *in vitro* studies[29]. *I41T* mutation has been hypothesized to produce some functional FIG4 proteins that would moderate the disease[30]. This hypothesis was tested here; the FIG4 level in this case was comparable to other cases in the group with teenage onset. This finding suggests that any compensation effect from I41T would be minimal.

Our previous study has shown that abnormal lysosomal storage in FIG4 deficient mouse fibroblasts was mainly caused by a lysosomal fission defect while lysosomal fusion was normal[11]. We verified this mechanism in five patients with CMT4J. After lysosomes were enlarged by application of Vacuolin-1 (5μM), lysosomal sizes gradually decreased via fission. This recovery was found to be highly abnormal in four cases (early onset + teenage onset). As expected, the recovery in case 3 (adult onset with high level of FIG4 and normal strength) was close to that in normal controls (Figure 2F).

Together, these findings support the loss-of-function of FIG4 in all 12 cases, including six cases with novel pathogenic mutations. The FIG4 deficiency also resulted in lysosomal fission defect in human cells.

Segmental demyelination was found in sciatic nerves from *Fig4*$^{-/-}$ mice

To understand the mechanisms of demyelination in CMT4J, we characterized segmental demyelination in *Fig4*$^{-/-}$ mice. A previous study has documented segmental demyelination in a set of *Fig4*$^{-/-}$ mice near their terminal stage (p42)[14]. Here, we examined this issue at postnatal day 21 (p21) of age. Again, there was a significant reduction of CV in *Fig4*$^{-/-}$ sciatic nerves, compared with that in *Fig4*$^{+/+}$ mice (Figure 3A–B; 17.6±3.3 m/s for n = 5 *Fig4*$^{+/+}$ mice vs. 7.8±1.9 m/s for n = 6 *Fig4*$^{-/-}$ mice; $p<0.01$). On teased nerve fiber preparation of sciatic nerves, we found segmental demyelination in 14.3±1.3% of fibers in *Fig4*$^{-/-}$ mice but only 1.9±1.6% in wild-type mice ($p<0.01$; n=3 mice for each genotypic group).

Remyelinated internodes after demyelination are usually shortened. We thus quantified internodal length and confirmed shorter internodes in *Fig4*$^{-/-}$ mice, in comparison with that in *Fig4*$^{+/+}$ mice (Figure 3C–F). Shortened internodes mainly affected large diameter fibers rather than small diameter fibers (Figure 3E).

Schwann cells in *Fig4*$^{-/-}$ mice showed increased dedifferentiation induced by abnormally elevated intracellular Ca^{2+}

Studies in either inherited or acquired dys-/demyelinating neuropathies have demonstrated an increase of Schwann cell dedifferentiation, which may play a role in demyelination. c-Jun has been one of the best documented dedifferentiation factors involved in the process[31,32]. Immunostaining of mouse sciatic nerves showed increased c-Jun in *Fig4*$^{-/-}$ mice, but c-Jun was barely present in *Fig4*$^{+/+}$ mice (Figure 4A–H). In teased nerve fiber preparation, the Schwann cell nuclei that stained positively for c-Jun were consistently correlated with segmental demyelination (Figure 4I–Q). The increase of nuclear c-Jun was found even in partially demyelinated internodes (Figure 4L–N).

Next, we quantified a battery of dedifferentiation factors using Western blot (Figure 5A–B). Indeed, c-Jun, phosphorylated c-Jun (pc-Jun) and p75 were robustly increased in *Fig4*$^{-/-}$ nerves. In contrast, factors for promoting myelination, such as Sox10 and Egr2, did not show significant changes in *Fig4*$^{-/-}$ mice. By real-time PCR, mRNA level of *c-Jun* was increased in *Fig4*$^{-/-}$ sciatic nerves, compared to *Fig4*$^{+/+}$ nerves (c-Jun: 0.9±0.1 in 4 *Fig4*$^{-/-}$ mice vs. 0.3±0.1 in 4 *Fig4*$^{+/+}$ mice, $p<0.001$; pc-Jun: 0.6±0.2 in *Fig4*$^{-/-}$ mice vs. 0.1±0.0 in *Fig4*$^{+/+}$ mice, $p<0.01$). Notch-1 was marginally increased and thus, was not studied further (0.9±0.1 in 4 *Fig4*$^{-/-}$ mice vs. 0.7±0.0 in 4 *Fig4*$^{+/+}$ mice; $p=0.048$).

Our previous study has demonstrated an increase of Ca^{2+} levels in *Fig4*$^{-/-}$ cells, including Schwann cells[11]. We hypothesized that the increase of intracellular Ca^{2+} may have stimulated overexpression of c-Jun. After applying a Ca^{2+} ionophore (A23187) capable of penetrating cell membrane into Schwann cells, c-Jun levels were increased both *in vitro* and *in vivo* (Figure 5C–D). In contrast, application of Ca^{2+} chelator (BAPTA) in cultured Schwann cells reduced c-Jun levels (Figure 5E–F). Injection of BAPTA (subcutaneously, daily) over 7 days also decreased c-Jun levels in *Fig4*$^{-/-}$ mouse sciatic nerves (Figure 5F).

Together, these findings support an increase of dedifferentiation in *Fig4*$^{-/-}$ Schwann cells through overexpression of c-Jun induced by abnormally elevated intracellular Ca^{2+}.

Macrophages were increased in the peripheral nerves of *Fig4*$^{-/-}$ mice

Increased abundance of inflammatory cells is usually a prominent feature in acquired demyelinating polyneuropathies but may occur in inherited peripheral nerve diseases. Furthermore, we have noticed macrophages containing phagocytosed myelin debris in *Fig4*$^{-/-}$ spinal roots under electron microscopy in our previous study[14]. We quantified macrophages in p21 mice by staining nerves with macrophage specific CD68 antibodies (Figure 5G). There was a robust increase of macrophages in *Fig4*$^{-/-}$ spinal roots but not in sciatic nerves. This localization mirrors what has been found in acquired demyelinating neuropathies where inflammatory cells are localized in areas with weak blood-nerve barriers including spinal roots. This CD68 increase was associated with an increase of Schwann cells stained positively for c-Jun in spinal roots. However, similar association was not found in sciatic nerves. CD68 was not increased in sciatic nerves where Schwann cells positive for c-Jun were still increased (Figure 5H). These findings do not support macrophage as a direct cause of increase of c-Jun expression in Schwann cells.

Demyelination in FIG4 deficiency results from abnormal interactions of multiple cell types

The increase of macrophages in *Fig4*$^{-/-}$ nerves prompted the important question of whether demyelination was due to the FIG4 deficiency solely in Schwann cells. We thus inserted two *LoxP* sites to flank the exons 2 and 3 in mouse *Fig4* (*Fig4*$^{f/f}$) (Figure 6A). The *Fig4*$^{f/f}$ mouse was crossed with a *Mpz*^{cre} mouse to produce a Schwann cell specific conditional knockout (*scFig4*$^{-/-}$) (Figure 6B). There was no significant increase of segmental demyelination in *scFig4*$^{-/-}$ mice by teased nerve fiber analysis (1.5±0.6% for 4 *Fig4*$^{f/f}$ mice vs. 1.2±0.4 for *scFig4*$^{-/-}$ mice at 9 months of age; $p>0.5$). In line with this finding, g-ratio of myelinated nerve fibers was similar between *Fig4*$^{f/f}$ and *scFig4*$^{-/-}$ mice (Figure 6C–D). Instead, there was a late-onset axonal loss at 9 months of age in *scFig4*$^{-/-}$ mice (Figure 6E–J).

Next, we produced the neuron-specific knockouts (*nFig4*$^{-/-}$) by crossing *Fig4*$^{f/f}$ mice with neuron-specific synapsin-cre mice (*Syn*^{cre}). Percentages of nerve fibers with segmental demyelination were similar between *Fig4*$^{f/f}$ and *nFig4*$^{-/-}$ mice (0.9±0.8% for three *Fig4*$^{f/f}$ mice vs. 1.0±0.7 for 4 *nFig4*$^{-/-}$mice at three months of age; $p>0.5$).

These observations strongly suggest that segmental demyelination resulted from contributions of multiple cell types. Successful therapy would not be achieved by targeting a single cell population but would require systemic delivery. BAPTA-AM has been used systemically (i.p.) in mice[33]. BAPTA suppressed c-Jun levels in *Fig4*$^{-/-}$ mouse sciatic nerves shown in Figure 5. Therefore, for proof-of-concept, we performed a trial of systemic BAPTA delivery in *Fig4*$^{-/-}$ mice (subcutaneous injection). Due to potential toxicity, a low dose (5mg/kg; concentration 0.5mg/ml) was used. Based on the variability of segmental demyelination counted on teased nerve fibers, our power calculation showed five mice (at p21 of age) per group would allow an 86% of chance to detect a significant difference. Five mice were randomized into three groups – BAPTA treated, vehicle (DMSO), and saline (to exclude effect from DMSO). Outcome measurement was done by experimenters that were blinded to the treatment groups. There was a significant reduction of demyelinated nerve fibers in the BAPTA treated group in comparison with the DMSO and saline group (saline 11.9±1.0% vs. DMSO 8.7±2.4% vs. BAPTA 5.2±1.6%; $p<0.05$).

Discussion

CMT4J is an ultra-rare disease, and twelve patients with this genetic condition constitute a large cohort. Phenotypic analysis shows that segmental demyelination is a highly consistent feature. These findings strongly indicate a critical dependence of FIG4 for the normal functions of peripheral nerve myelin. This is consistent with the high level expression of FIG4 in Schwann cells[22].

The natural history of our patients disputes two previous speculations. First, CNS phenotypes in a subset of patients with CMT4J are suspected to relate to more severe depletion of FIG4[30]. However, patients with early onset and severe CNS abnormalities (#4 and #5) had levels of FIG4 similar to those patients with teenage onset (Figure 2). Instead, second mutations were found in the two cases with early onset. Because there are only two cases here, a causal relationship still cannot be established between CNS abnormalities and the 2nd mutations. However, the two 2nd mutations have been associated with neurological phenotypes. After all, it is well known that phenotypic variations in monogenic diseases can be caused by additional genetic modifiers[34]. Another speculation was that minor trauma triggers acceleration of disease progression[14]. However, surgeries in four patients and trauma in one case did not result in rapid disease progression. Instead, a majority of our CMT4J patients presented with relatively symmetric distal>proximal weakness and sensory deficits in limbs. In addition, while all CMT4J mutations resulted in FIG4 deficiency, the levels of FIG4 could not differentiate patients with early onset from those with teenage onset. Thus, other intrinsic and extrinsic factors (not necessarily trauma) may have been involved in the modification of CMT4J phenotype.

We believe that the consistent pathology of segmental demyelination in CMT4J is highly significant for the following reasons. First, demyelination in patients with CMT4J and *Fig4*$^{-/-}$ mouse models recapitulates many features typically seen in acquired demyelinating peripheral nerve disorders, including conduction block, temporal dispersion, non-uniform slowing on NCS and macrophage increase in areas with weak blood-nerve barrier. The demyelination appears to be primary. For instance, in case #9 and #10, most motor nerves in arms had normal amplitudes of CMAP, but conduction velocities were still very much decreased (Table 1B). Some acquired demyelinating features have also been reported in a subset of patients with CMTX1[35] and a heterozygous *myelin protein zero* knockout mouse (*Mpz*$^{+/-}$)[36]. Thus, studies of these diseases may reveal novel molecular pathways potentially relevant to many demyelinating diseases. Indeed, there have been many precedent examples showing that acquired or sporadic diseases can be studied by utilizing genetic models derived from inherited disorders. In the field of ALS, a variety of rodent genetic models, such as the *C9ORF72, SOD1* and *TDP43* transgenic mice, have been used to study the pathogenic mechanisms of the disease. While ALS patients with mutations in *C9ORF72, SOD1* or *TDP43* are rare, investigations using these genetically manipulated animals have made remarkable contributions to our understanding of the pathogenesis of ALS in general[37,38]. Thus, similar advances in acquired demyelinating diseases could be achieved through the use of CMT4J genetic models.

Second, Schwann cell dedifferentiation and intracellular Ca^{2+} elevation have been suggested to play roles in segmental demyelination[32,39]. However, the relationship between c-Jun and Ca^{2+} remains unclear. It is also unclear if the increase of c-Jun and/or intracellular Ca^{2+} directly causes segmental demyelination. Our results suggest that a high Ca^{2+} level in *Fig4*$^{-/-}$ cells likely leads to the increase of c-Jun since application of exogenous Ca^{2+} increases c-Jun and a suppression of endogenous Ca^{2+} decreases c-Jun (Figure 5C–F).

Third, chelation of excessive Ca^{2+} in *Fig4*$^{-/-}$ mice improved segmental demyelination, supporting the contribution of Ca^{2+} to segmental demyelination. This finding is in line with observations from other studies showing the contribution of high Ca^{2+} to demyelination in inherited and acquired demyelinating neuropathy models and the rescue of segmental demyelination by blocking excessive Ca^{2+} released from mitochondria in Schwann cells[39,40]. However, it is still uncertain if excessive Ca^{2+} in *Fig4*$^{-/-}$ mice causes segmental demyelination through the increase of c-Jun. Nevertheless, these observations suggest a different approach to the treatment of demyelination.

To our surprise, segmental demyelination in FIG4 deficiency is not a cell autonomous process of Schwann cells. This observation is instrumental to future therapeutic development, since treatment targeting single cell population is unlikely to be effective; instead, a systemic delivery to reach multiple cell population is required. This notion is also in line with previous observations that excessive lysosomal storages were found in multiple cell types and organs (peripheral nerves, oligodendrocytes, CNS neurons, spinal motor neurons, DRG neurons, skin fibroblasts, spleen cells)[9,14], supporting a systemic disease of CMT4J.

It is not clear exactly how FIG4-deficient axons or macrophages contribute to segmental demyelination. One potential mechanism to be tested in the future is that axons or macrophages with FIG4 deficiency may elevate Ca^{2+} levels further or trigger more Ca^{2+} release from lysosomes in *Fig4*$^{-/-}$ Schwann cells. Because Ca^{2+} is already increased in *Fig4*$^{-/-}$ Schwann cells[11], a further increase of cytosolic Ca^{2+} level likely initiates a cascade of events leading to demyelination[39]. In line with this idea, axonal damage has been shown to increase intracellular Ca^{2+} level in myelin[41]. It is also interesting to note that depletion of macrophages by the treatment of CSF1R receptor inhibitor improved pathology in two inherited neuropathy mouse models[42].

It should be clarified that our findings do not exclude developmental abnormality of myelin (**dys**myelination) in CMT4J. For instance, we observed shortened internodes in *Fig4*$^{-/-}$ mice (Figure 3). One could argue that this change could reflect a failure of *Fig4*$^{-/-}$ Schwann cells reaching normal internodal length during development. While this is possible, it cannot be the sole pathology responsible for the slowed CV in *Fig4*$^{-/-}$ mice. A previous study has elegantly demonstrated that a 50% reduction of internodal length results in a CV about one half of normal[43]. Internodal length in *Fig4*$^{-/-}$ nerves was only decreased by 13% (Figure 3C–F). Thus, >50% reduction (Figure 3A–B) of CV in *Fig4*$^{-/-}$ nerves would have to be caused by additional factors, including segmental **de**myelination. Any **dys**myelination in *Fig4*$^{-/-}$ nerves would be a partial or a mild change.

With great interest, we noticed a late-onset and progressive axonal loss in Schwann cell conditional knockouts (*scFig4*$^{-/-}$ in Figure 6), suggesting that abnormal signals from FIG4 deficient Schwann cells instruct wild-type axons to degenerate. While not a focus of the present study, it would be of neurobiological significance to unveil any such abnormal signals.

In summary, our study strongly supports a critical role of FIG4 in peripheral nerve myelin. Our observation enables us to propose a mechanistic model (Figure 7) to be further tested. While our previous study has shown an increase of intracellular Ca^{2+} in *Fig4*$^{-/-}$ Schwann cells[11], this abnormality is likely further worsened by unidentified signals from axons and/or macrophages with FIG4 deficiency. Under the drive of multiple cell types depleted of FIG4, abnormally increased Ca^{2+} inside Schwann cells may reach a critical level resulting in demyelination either through dedifferentiating effect of c-Jun and/or other unknown pathways.

Acknowledgments

This research is supported by grants from Depart of Veterans Affairs (IBX003385A), NINDS (R01NS066927), the Muscular Dystrophy Association and the National Center for Advancing Translational Sciences (UL1TR000445; U54NS065712). Authors wish to thank Dr. Lily Wang for her assistance in statistics.

References

1. Gabreels-Festen AA, Bolhuis PA, Hoogendijk JE, et al. Charcot-Marie-Tooth disease type 1A: morphological phenotype of the 17p duplication versus PMP22 point mutations. Acta Neuropathol. 1995; 90:645–649. [PubMed: 8615087]
2. Lewis RA, Sumner AJ, Shy ME. Electrophysiological features of inherited demyelinating neuropathies: A reappraisal in the era of molecular diagnosis. Muscle Nerve. 2000; 23:1472–1487. [PubMed: 11003782]
3. Li J. Molecular Regulators of Nerve Conduction - Lessons from Inherited Neuropathies and Rodent Genetic Models. Exp Neurol. 2015
4. Jin N, Chow CY, Liu L, et al. VAC14 nucleates a protein complex essential for the acute interconversion of PI3P and PI(3,5)P(2) in yeast and mouse. EMBO J. 2008; 27:3221–3234. [PubMed: 19037259]
5. Ikonomov OC, Sbrissa D, Ijuin T, et al. Sac3 is an insulin-regulated phosphatidylinositol 3,5-bisphosphate phosphatase: gain in insulin responsiveness through Sac3 down-regulation in adipocytes. J Biol Chem. 2009; 284:23961–23971. [PubMed: 19578118]
6. Sbrissa D, Ikonomov OC, Fu Z, et al. Core protein machinery for mammalian phosphatidylinositol 3,5-bisphosphate synthesis and turnover that regulates the progression of endosomal transport. Novel Sac phosphatase joins the ArPIKfyve-PIKfyve complex. J Biol Chem. 2007; 282:23878–23891. [PubMed: 17556371]
7. Huotari J, Helenius A. Endosome maturation. EMBO J. 2011; 30:3481–3500. [PubMed: 21878991]
8. Chow CY, Zhang Y, Dowling JJ, et al. Mutation of FIG4 causes neurodegeneration in the pale tremor mouse and patients with CMT4J. Nature. 2007; 448:68–72. [PubMed: 17572665]
9. Katona I, Zhang X, Bai Y, et al. Distinct pathogenic processes between Fig4-deficient motor and sensory neurons. Eur J Neurosci. 2011; 33:1401–1410. [PubMed: 21410794]
10. Dong XP, Shen D, Wang X, et al. PI(3,5)P(2) Controls Membrane Traffic by Direct Activation of Mucolipin Ca Release Channels in the Endolysosome. Nat Commun. 2010; 1
11. Zou J, Hu B, Arpag S, et al. Reactivation of Lysosomal Ca2+ Efflux Rescues Abnormal Lysosomal Storage in FIG4-Deficient Cells. J Neurosci. 2015; 35:6801–6812. [PubMed: 25926456]

12. Brunden KR, Poduslo JF. Lysosomal delivery of the major myelin glycoprotein in the absence of myelin assembly: posttranslational regulation of the level of expression by Schwann cells. J Cell Biol. 1987; 104:661–669. [PubMed: 2434515]
13. Chen G, Zhang Z, Wei Z, et al. Lysosomal exocytosis in Schwann cells contributes to axon remyelination. Glia. 2012; 60:295–305. [PubMed: 22042600]
14. Zhang X, Chow CY, Sahenk Z, et al. Mutation of FIG4 causes a rapidly progressive, asymmetric neuronal degeneration. Brain. 2008; 131:1990–2001. [PubMed: 18556664]
15. Gentil BJ, O'Ferrall E, Chalk C, et al. A New Mutation in FIG4 Causes a Severe Form of CMT4J Involving TRPV4 in the Pathogenic Cascade. J Neuropathol Exp Neurol. 2017; 76:789–799. [PubMed: 28859335]
16. Murphy SM, Herrmann DN, McDermott MP, et al. Reliability of the CMT neuropathy score (second version) in Charcot-Marie-Tooth disease. J Peripher Nerv Syst. 2011; 16:191–198. [PubMed: 22003934]
17. Li J, Krajewski K, Shy ME, et al. Hereditary neuropathy with liability to pressure palsy: the electrophysiology fits the name. Neurology. 2002; 58:1769–1773. [PubMed: 12084875]
18. Cornblath DR, Sumner AJ. Conduction block in neuropathies with necrotizing vasculitis. Muscle Nerve. 1991; 14:185–186. [PubMed: 1847992]
19. Hu B, Arpag S, Zhang X, et al. Tuning PAK Activity to Rescue Abnormal Myelin Permeability in HNPP. PLoS Genet. 2016; 12:e1006290. [PubMed: 27583434]
20. Hu B, Arpag S, Zuchner S, et al. A novel missense mutation of CMT2P alters transcription machinery. Ann Neurol. 2016; 80:834–845. [PubMed: 27615052]
21. Bai Y, Zhang X, Katona I, et al. Conduction block in PMP22 deficiency. J Neurosci. 2010; 30:600–608. [PubMed: 20071523]
22. Guo J, Ma YH, Yan Q, et al. Fig4 expression in the rodent nervous system and its potential role in preventing abnormal lysosomal accumulation. J Neuropathol Exp Neurol. 2012; 71:28–39. [PubMed: 22157617]
23. Zaimi A, Duval T, Gasecka A, et al. AxonSeg: Open Source Software for Axon and Myelin Segmentation and Morphometric Analysis. Front Neuroinform. 2016; 10:37. [PubMed: 27594833]
24. Chow CY, Landers JE, Bergren SK, et al. Deleterious variants of FIG4, a phosphoinositide phosphatase, in patients with ALS. Am J Hum Genet. 2009; 84:85–88. [PubMed: 19118816]
25. Osmanovic A, Rangnau I, Kosfeld A, et al. FIG4 variants in central European patients with amyotrophic lateral sclerosis: a whole-exome and targeted sequencing study. Eur J Hum Genet. 2017; 25:324–331. [PubMed: 28051077]
26. Cornblath DR, Sumner AJ, Daube J, et al. Conduction block in clinical practice. Muscle Nerve. 1991; 14:869–871. [PubMed: 1922183]
27. Adzhubei IA, Schmidt S, Peshkin L, et al. A method and server for predicting damaging missense mutations. Nat Methods. 2010; 7:248–249. [PubMed: 20354512]
28. Kumar P, Henikoff S, Ng PC. Predicting the effects of coding non-synonymous variants on protein function using the SIFT algorithm. Nat Protoc. 2009; 4:1073–1081. [PubMed: 19561590]
29. Ikonomov OC, Sbrissa D, Fligger J, et al. ArPIKfyve regulates Sac3 protein abundance and turnover: disruption of the mechanism by Sac3I41T mutation causing Charcot-Marie-Tooth 4J disorder. J Biol Chem. 2010; 285:26760–26764. [PubMed: 20630877]
30. Martyn C, Li J. Fig4 deficiency: A newly emerged lysosomal storage disorder? Prog Neurobiol. 2012
31. Jessen KR, Mirsky R. Negative regulation of myelination: relevance for development, injury, and demyelinating disease. Glia. 2008; 56:1552–1565. [PubMed: 18803323]
32. Jang SY, Yoon BA, Shin YK, et al. Schwann cell dedifferentiation-associated demyelination leads to exocytotic myelin clearance in inflammatory segmental demyelination. Glia. 2017; 65:1848–1862. [PubMed: 28795433]
33. Balino P, Monferrer L, Pastor R, et al. Intracellular calcium chelation with BAPTA-AM modulates ethanol-induced behavioral effects in mice. Exp Neurol. 2012; 234:446–453. [PubMed: 22306018]
34. Hightower RM, Alexander MS. Genetic modifiers of Duchenne and facioscapulohumeral muscular dystrophies. Muscle Nerve. 2018; 57:6–15. [PubMed: 28877560]

35. Gutierrez A, England JD, Sumner AJ, et al. Unusual electrophysiological findings in X-linked dominant Charcot-Marie-Tooth disease. Muscle Nerve. 2000; 23:182–188. [PubMed: 10639608]
36. Shy ME, Arroyo E, Sladky J, et al. Heterozygous P0 knockout mice develop a peripheral neuropathy that resembles chronic inflammatory demyelinating polyneuropathy (CIDP). J Neuropathol Exp Neurol. 1997; 56:811–821. [PubMed: 9210878]
37. Swarup V, Julien JP. ALS pathogenesis: Recent insights from genetics and mouse models. Prog Neuropsychopharmacol Biol Psychiatry. 2010
38. Chew J, Gendron TF, Prudencio M, et al. Neurodegeneration. C9ORF72 repeat expansions in mice cause TDP-43 pathology, neuronal loss, and behavioral deficits. Science. 2015; 348:1151–1154. [PubMed: 25977373]
39. Gonzalez S, Berthelot J, Jiner J, et al. Blocking mitochondrial calcium release in Schwann cells prevents demyelinating neuropathies. J Clin Invest. 2017; 127:1115.
40. Nobbio L, Sturla L, Fiorese F, et al. P2X7-mediated increased intracellular calcium causes functional derangement in Schwann cells from rats with CMT1A neuropathy. J Biol Chem. 2009; 284:23146–23158. [PubMed: 19546221]
41. Yan JG, Matloub HS, Yan Y, et al. The correlation between calcium absorption and electrophysiological recovery in crushed rat peripheral nerves. Microsurgery. 2010; 30:138–145. [PubMed: 19790186]
42. Klein D, Patzko A, Schreiber D, et al. Targeting the colony stimulating factor 1 receptor alleviates two forms of Charcot-Marie-Tooth disease in mice. Brain. 2015; 138:3193–3205. [PubMed: 26297559]
43. Court FA, Sherman DL, Pratt T, et al. Restricted growth of Schwann cells lacking Cajal bands slows conduction in myelinated nerves. Nature. 2004; 431:191–195. [PubMed: 15356632]
44. Mironova YA, Lenk GM, Lin JP, et al. PI(3,5)P2 biosynthesis regulates oligodendrocyte differentiation by intrinsic and extrinsic mechanisms. Elife. 2016; 5
45. Lloyd-Evans E, Platt FM. Lysosomal Ca(2+) homeostasis: role in pathogenesis of lysosomal storage diseases. Cell Calcium. 2011; 50:200–205. [PubMed: 21724254]
46. Pitt SJ, Funnell TM, Sitsapesan M, et al. TPC2 is a novel NAADP-sensitive Ca2+ release channel, operating as a dual sensor of luminal pH and Ca2+ J Biol Chem. 2010; 285:35039–35046. [PubMed: 20720007]

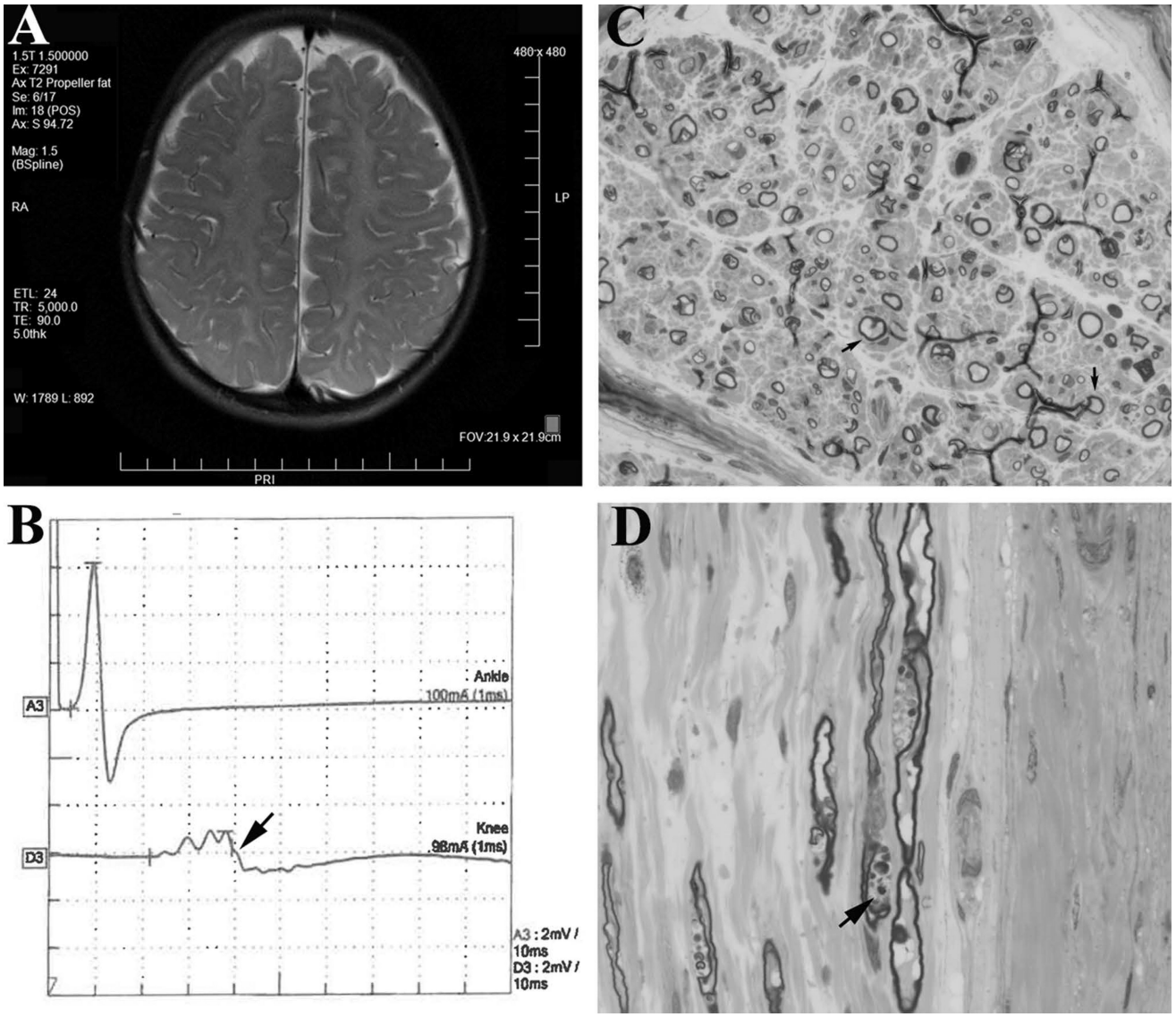

Figure 1.

(A). A T2 weighted brain MRI from Case #5 at 4 years of age showed white matter changes, presumably due to hypomyelination[44]. (B). NCS of tibial motor nerve in Case #3 revealed temporal dispersion (arrow) evoked by proximal stimulation. (C). Transverse semithin section of the Case #5's sural nerve (63× lens; biopsied at 14 months of age) was stained by Toluidine blue and demonstrated a severe reduction of large myelinated nerve fibers. The remaining large fibers showed thin myelin. Onion bulbs were present (arrows). (D). Longitudinal section of the same sural nerve (63× lens) revealed myelin debris (arrow).

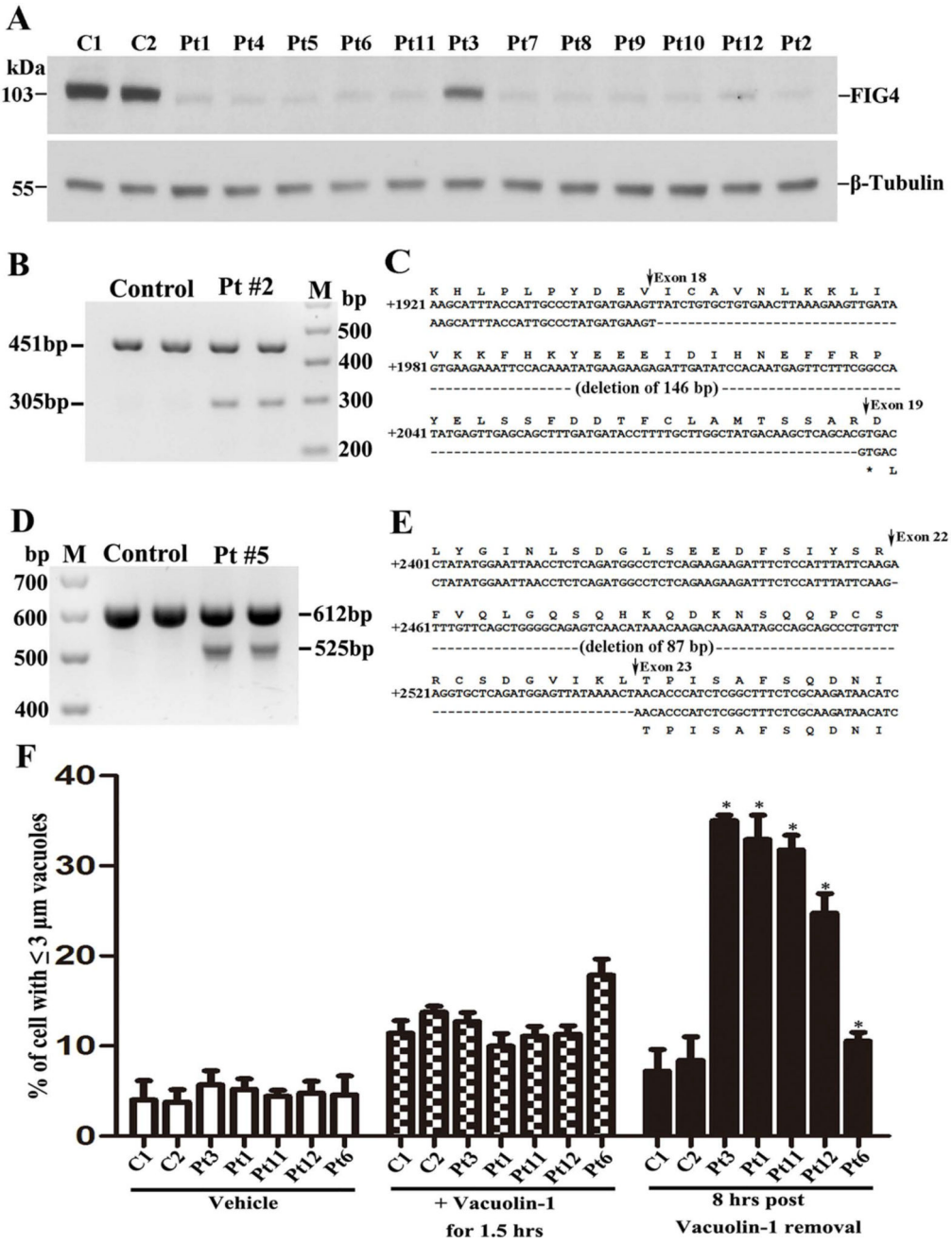

Figure 2.

(A). Western blot analysis of FIG4 was performed on the protein lysates extracted from the fibroblasts of normal controls and patients. The levels of FIG4 were either absent or severely decreased in all CMT4J patients. β-Tubulin - loading control. C = control; Pt = Patient (= case #). (B). RT-PCR products amplified in RNA from the fibroblasts of 2 controls and case #2. The band of 451bp was the normal *FIG4* allele transcript. The smaller band of 305bp was the misspliced *FIG4* transcript. M = DNA marker. (C). Sequence comparison between normal and mutant allele showed loss of exon 18. (D). In case #5, but not the normal control, two RT-PCR products were detected: 612bp was the normal *FIG4* transcript, and a shorter

band of 525bp was from the skipping of exon 22. (E). Sequence comparison between normal and mutant alleles showed deletion of exon 22. (F). Fibroblasts from 2 normal controls and case 3, 1, 11, 12, and 6 were analyzed for their lysosomal fission as described in Methods. The cells were exposed to Vacuolin-1 for 1.5 hours and imaged, followed by washing with culture media. The cells were imaged again at the 8^{th} hour after the wash-out. Percentages of cells with lysosomal vacuoles ≥3μM in diameters were counted in the images. * = statistically significant with p value < 0.05.

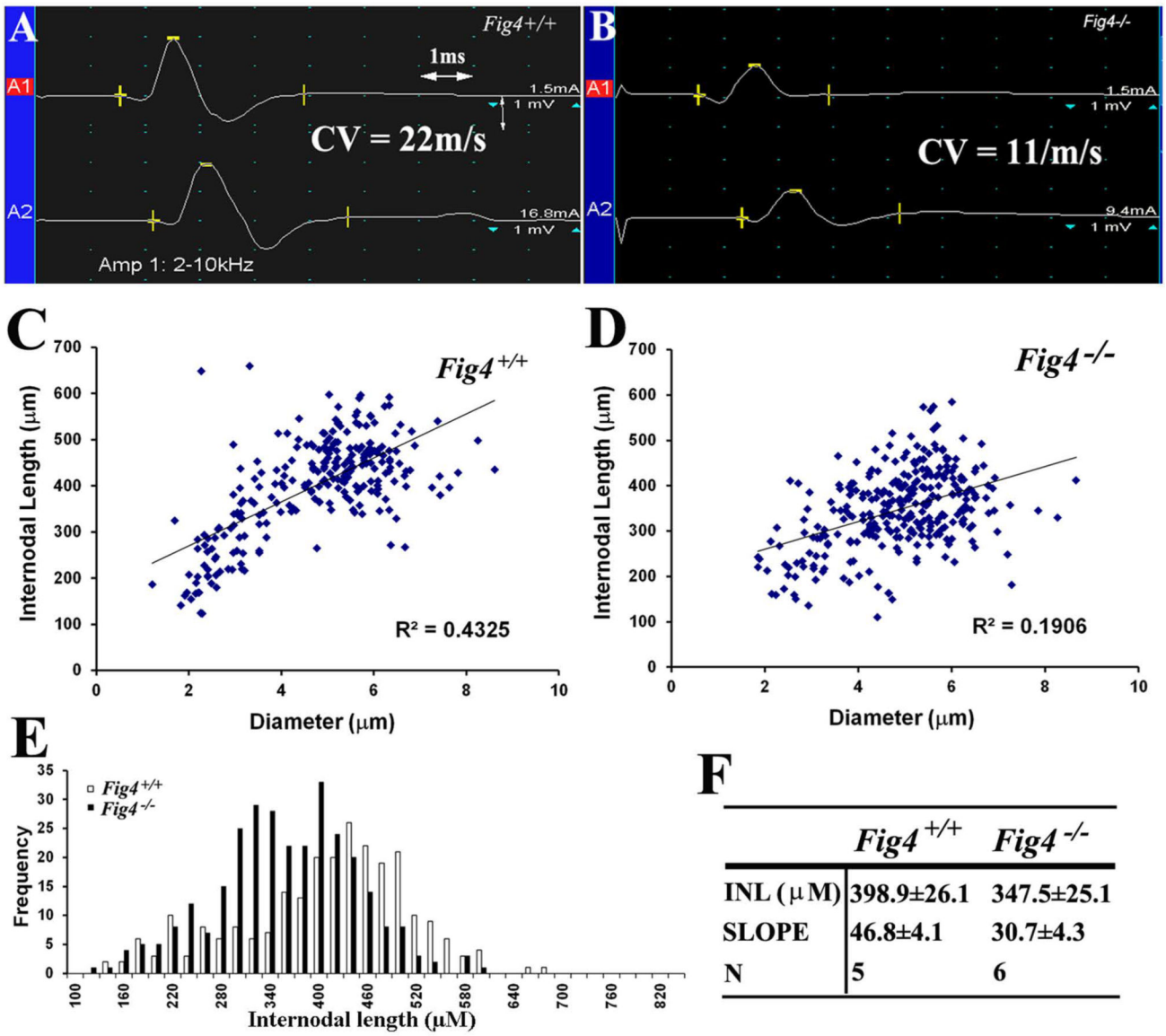

Figure 3.

(A). Compound muscle action potential (CMAP) was recorded from a p21 *Fig4*$^{+/+}$ mouse paw. The motor nerve conduction velocity (CV) was 22m/s. (B). The same experiment was done in a p21 *Fig4*$^{-/-}$ mouse and showed a 50% reduction of CV. (C–D). Mouse sciatic nerves were teased into individual fibers in liquid Epon and imaged. Internodal length and diameter were measured and plotted. The slope in *Fig4*$^{-/-}$ mice was lower than that in *Fig4*$^{+/+}$ mice, supporting shortened internodal length in *Fig4*$^{-/-}$ mice. (E). The frequency vs. diameter plot allows a better visualization of shortened internodes mainly involving those longest (largest) fibers. (F). INL = internodal length; N = number of mice; $p<0.05$ for the comparison of both internodal length and slope.

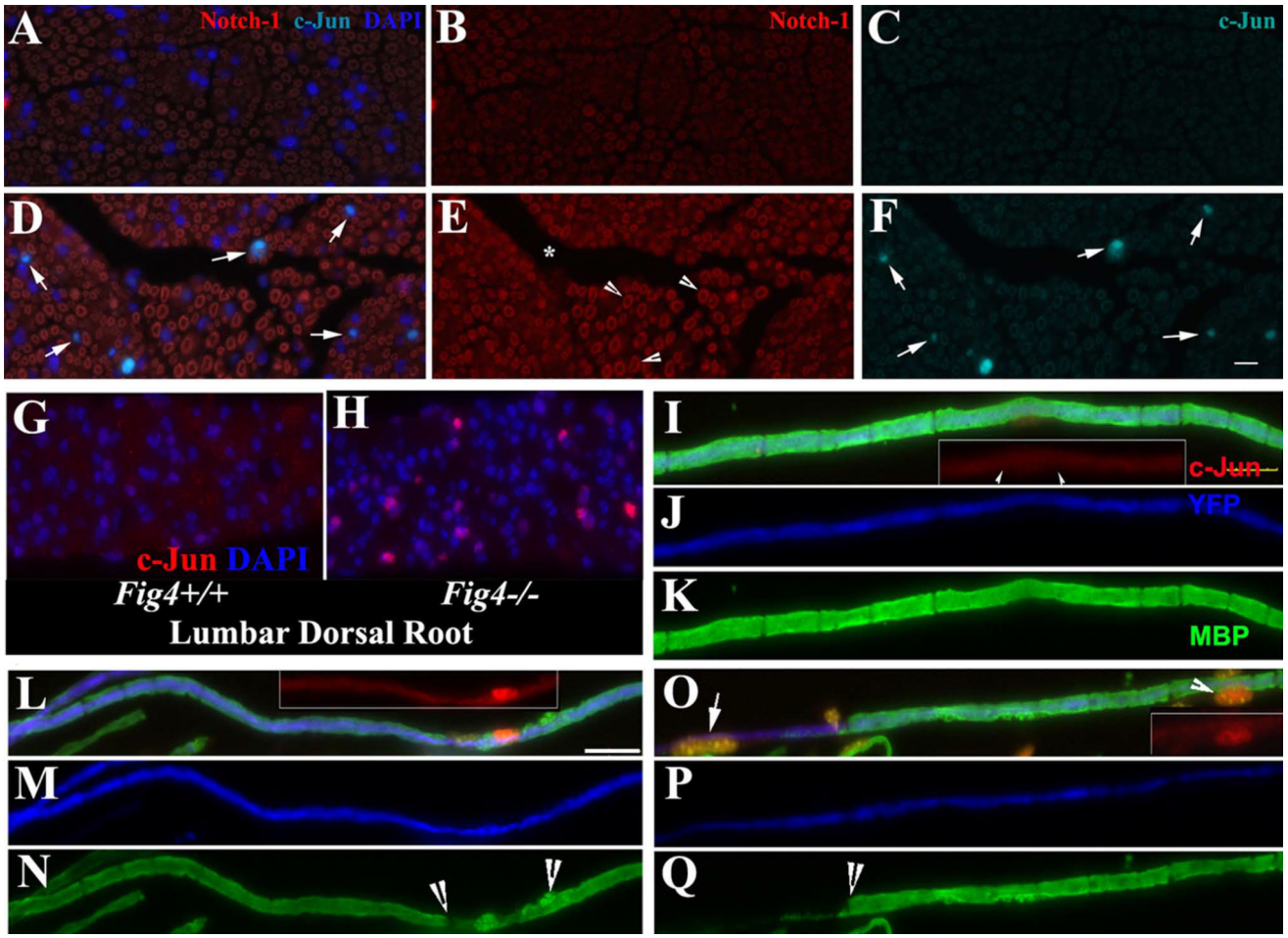

Figure 4.

(A–F). A, B and C are for *Fig4*$^{+/+}$ nerves. D, E and F are for *Fig4*$^{-/-}$ nerves. Transverse sections of adult mouse sciatic nerves were stained with antibodies against c-Jun and Notch-1. In line with previous studies, Notch-1 was localized in myelin (A, B, D, and E). F. There was an increase of c-Jun in the Schwann cell nuclei of *Fig4*$^{-/-}$ nerves, compared with that in *Fig4*$^{+/+}$ nerves in C. (G–H). There were numerous nuclei in *Fig4*$^{-/-}$ spinal roots showing strong c-Jun signal, which was hardly seen in *Fig4*$^{+/+}$ spinal roots. (I–K). A wild-type myelinated nerve fiber from a sciatic nerve was stained with antibodies against c-Jun and MBP (which labels myelin). The axon was labeled with YFP (artificially changed to blue color) expressed under a neuronal specific promoter. c-Jun staining was hardly visible in the nucleus (arrowheads in inset). (L–N). A *Fig4*$^{-/-}$ sciatic nerve fiber with subtle demyelination (between arrowheads in N) showed a robust increase of c-Jun (inset in L) in the Schwann cell nucleus. (O–Q). The increase of c-Jun (inset in O) was seen in a *Fig4*$^{-/-}$ sciatic nerve fiber with severe segmental demyelination (left to arrow in Q). The Schwann cell nucleus at the middle of the internode (arrowhead in O and inset in O) showed an increased c-Jun. Another nucleus in the demyelinated region also expressed a high level of c-Jun (arrow in O). Scale bars = 10μm

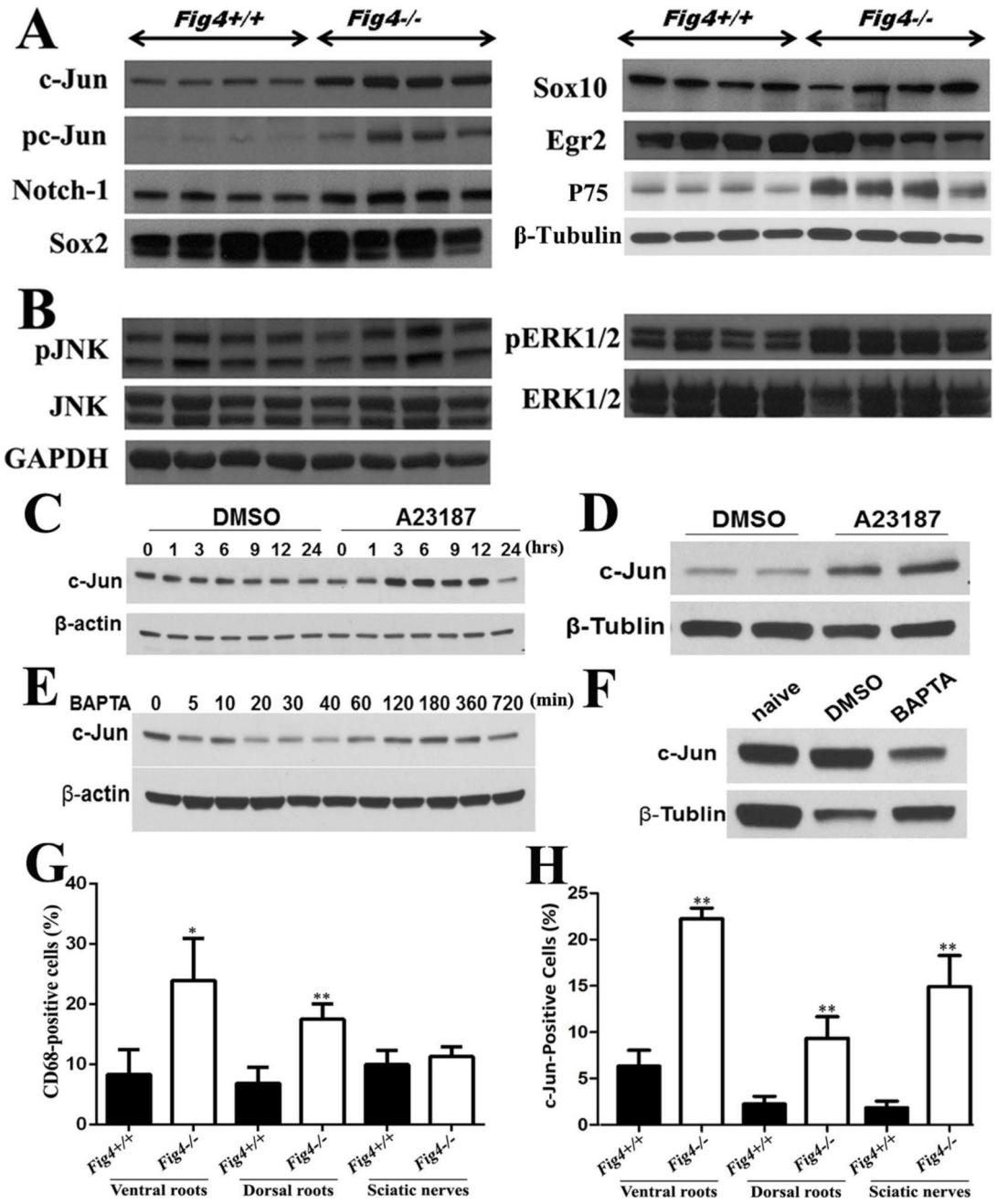

Figure 5.

(A). Mouse sciatic nerves at the age of p21 days were studied by Western blot. c-Jun, p75 and phosphorylated c-Jun (pc-Jun) were robustly increased in *Fig4*$^{-/-}$ mice. Notch-1 was marginally increased (p=0.048). Sox10 and Egr2 did not show significant changes in *Fig4*$^{-/-}$ mice. (B). Molecules up-stream and down-stream to c-Jun were also evaluated in *Fig4*$^{-/-}$ mice. GAPDH = loading control. (C). Schwann cells in culture were treated with Ca^{2+} ionophore A23187 (2.5μM). c-Jun levels were increased after 1 hour. There were numerous cells dead at 24 hours, leading a decrease of c-Jun level. (D). Sciatic nerves in wild-type mice were surgically exposed and wrapped by gauzes soaked with 19μM A23187 for 4

hours. Nerves were then dissected for Western blot analysis to measure c-Jun levels. (E). Schwann cells were incubated with BAPTA (30μM). Protein lysates were extracted from the cells at different time points for Western blot. (F). Two wild-type mice were treated with either vehicle or BAPTA (5mg/kg; i.p. daily) for 7 days. A naïve mouse was used for control. Sciatic nerves were then collected for Western blot analysis. (G). Transverse section of paraffin embedded mouse nerves at p21 of age was stained with antibodies against CD68. The increase of CD68 was robust in spinal roots of *Fig4*$^{-/-}$ mice but was not seen in the sciatic nerves. (H). When c-Jun was stained, its increase was found in all parts of peripheral nerves. * = $P< 0.05$, ** = $P< 0.01$

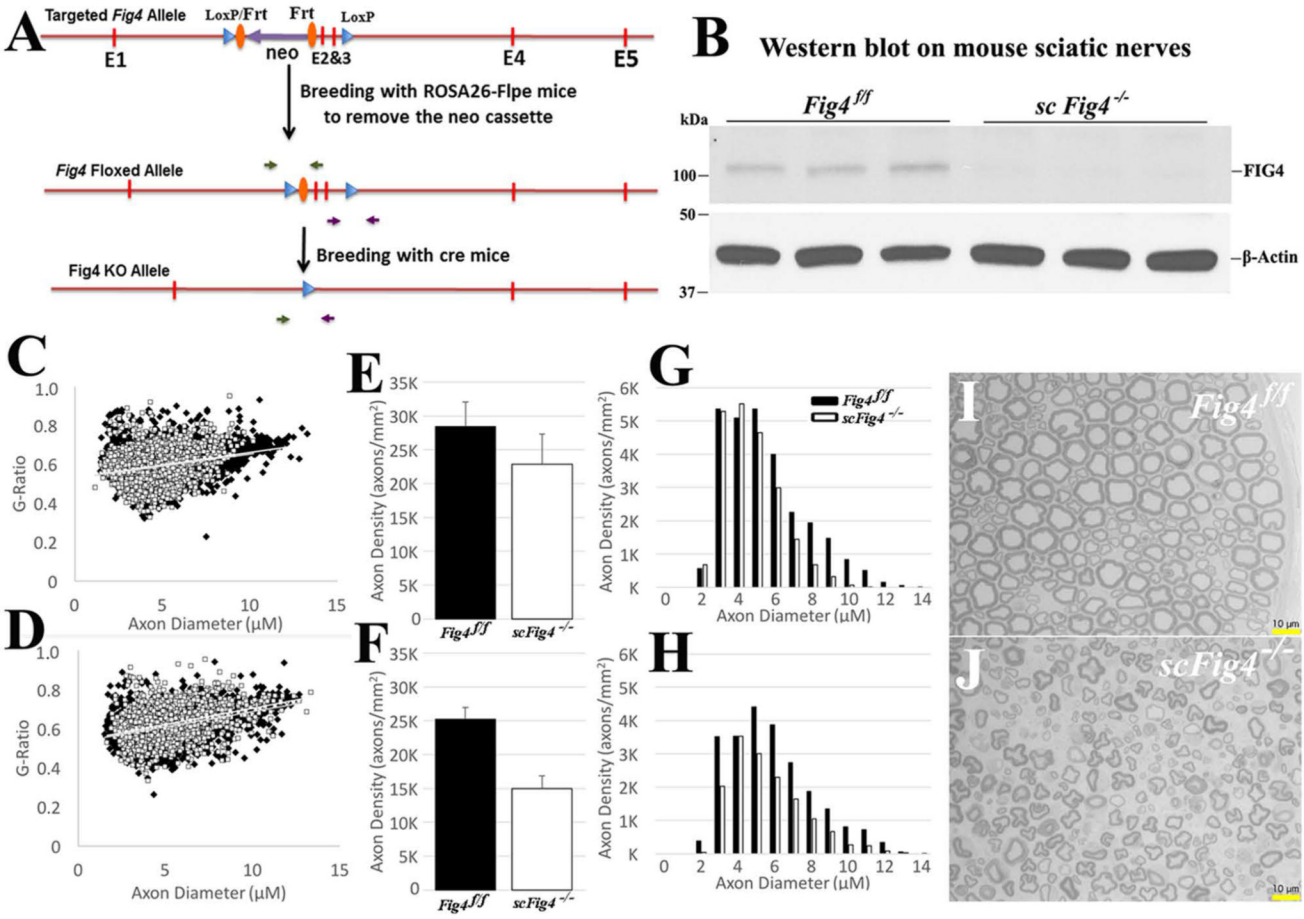

Figure 6.

(A). *Fig4* targeting vector was prepared by retrieving 8.8 kb of *Fig4* containing exons 2–3 from BAC (RP24-96F12) into PL253 containing the HSV-TK negative selectable marker by gap repair. The 5'LoxP site was inserted 600bp 3' of exon 3 followed by insertion of the Frt-PGKneo-Frt-LoxP cassette 450bp 5' of exon 2. The final vector contains 5' and 3' arms of 4.9 and 3.4 kb respectively. The vector was then linearized and electroporated into mouse ES cells derived from F1 (129Sv/C57BL6/J) blastocyst. Electroporated cells were cultured in the presence of G418 and Gancyclovir for 48 hours. PCR using primers corresponding to sequences outside the arms and to the 5' and 3' LoxP sites identified the targeted ES clones. Expanded ES colonies were used to generate chimeric animals by ES/morula aggregation. Chimeric animals were bred with ROSA26-Flpe mice (Jax stock no: 003946) to remove the PGKneo cassette to generate the final conditional knockin mice ($Fig4^{f/f}$). (B). $Fig4^{f/f}$ mice were crossed with Mpz^{cre} mice to produce Schwann cell-specific knockout mice ($scFig4^{-/-}$). At p21, sciatic nerves were dissected for Western blot with antibodies against FIG4. Note that non-Schwann cells would still express some FIG4 in $scFig4^{-/-}$ nerves. We stripped epineurium of sciatic nerves. This procedure resulted in a low concentration of total proteins. Nevertheless, FIG4 was readily detectable in $Fig4^{f/f}$ nerves, but hardly visible in $scFig4^{-/-}$ nerves. β-Actin - loading controls. (C–D). G-ratio was plotted against nerve fiber diameters in 4-month-old (C) and 9-month-old (D) mice. Slopes between $Fig4^{f/f}$ and $scFig4^{-/-}$ mice were nearly identical, suggesting comparable myelin thickness. (E–F). Axon

density decreased from 4-month-old (E) to 9-month-old (F) mice. (G–H). The axonal loss mainly affected large nerve fibers (G for 4-month-old; H for 9-month-old) when visualized using histogram. (I–J). Images of semithin section were taken from 9-month-old *Fig4*$^{f/f}$ (I) and *scFig4*$^{-/-}$ (J) mice. Notice that myelinated nerve fibers in *scFig4*$^{-/-}$ nerve were smaller with irregularity of myelin. However, there was no sign of demyelination, such as myelin debris, axons with broken myelin or absence of myelin.

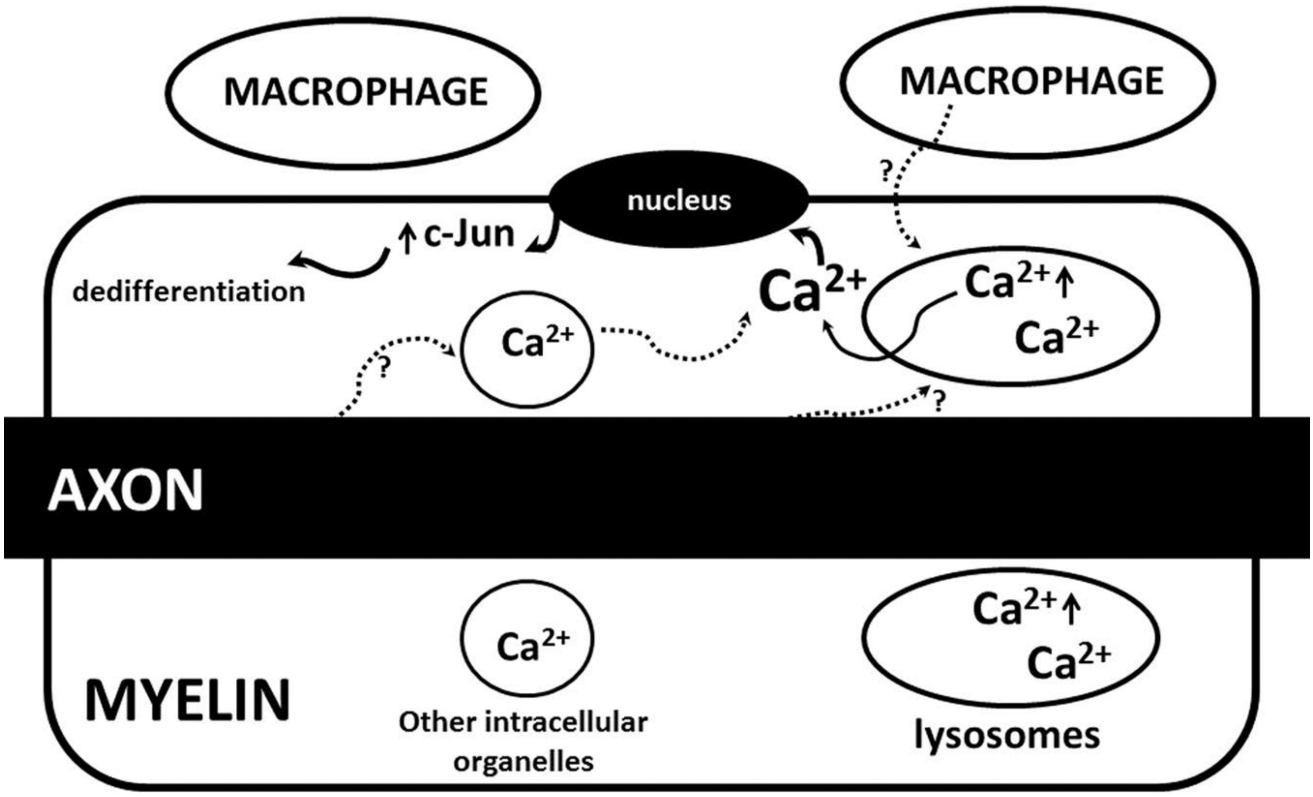

Figure 7.

A proposed mechanistic model to be further tested in the future: Release of Ca^{2+} from lysosome is primarily through two Ca^{2+} channels, TRPML1 and TPC2[45]. $PI3,5P_2$ binds with TRPML1 to activate Ca^{2+} efflux through TRPML1[10]. Since $PI3,5P_2$ is deficient in *Fig4*−/− cells, lysosomes develop a high level of Ca^{2+}. The extra Ca^{2+} in *Fig4*−/− lysosomes can be released by internal or external signals (speculated from axons or macrophages) to stimulate expression of dedifferentiation molecules like c-Jun, promoting demyelination. Excessive Ca^{2+} could also promote demyelination via other unidentified pathways.

Table 1

A. Phenotypes and Genotypes

	Age	Sex	Onset	Mutation	UE (D/P)[1]	LE (D/P)[2]	SF[3]	Trau[4]	CNS[5]	CMTES	F/U[6]
1	17	M	12	I41T/R432x*	4/5	4/5	dec[7]	no	no	9	no
2	52	F	12	I41T/IVS17-10+T>G[8]	1–3/5	1–2/5	dec	no	yes	13	n/a[9]
3	25	F	25	I41T/3bp del[10*]	5/5	5/5	dec	yes	no	2	no
4	11	F	birth	I41T/L458FfsX5	3/4	3/4	n/r[10]	no	yes	p34[11]	n/a
5	8	M	birth	K278fsX6/IVS21+1G>A[8*]	1/2	1/2	n/r	no	yes	n/a	n/a
6	34	F	14	I41T/F98Lfs	3/5	1–2/4	dec	yes	no	17	no
7	16	F	15	I41T/W246X*	4/5	4/5	dec	yes	no	11	no
8	14	M	12	I41T/W246X	5/5	5/5	nl[12]	yes	no	2	n/a
9	35	M	32	I41T/R183X	5/5	1/3	dec	no	no	12	no
10	37	F	13	I41T/R183X	1/4	0/1	dec	yes	no	16	n/a
11	6	M	birth	I41T/Exon8-10 del*	2/4	0/3	n/r	no	no	n/a	n/a
12	10	M	9	I41T/I41T*	4/5	4/5	nl[12]	no	no	2	n/a

B. Nerve conduction studies

	Sensory Nerves (DL/Amp/CV)[1]				Motor Nerves (DL/Amp/CV)				C/T[2]
	median	ulnar	radial	sural	median	ulnar	peroneal	tibial	
1	nr[3]	nr	nr	nr	24.4/3.3/7.0	nr	nr	nr	y/n
2	4.3/10.0/31.5	4.4/6.0/31.4	nr	nr	5.4/4.9/33.0	4.6/6.7/33.6	nr	na[4]	y/y
3	4.2/6.8/30.0	2.6/12.6/46.0	1.7/4.5/59.0	nr	4.9/8.4/29.0	3.2/7.3/39.0	4.7/4.9/21.0	4.5/6.9/29.0	y/y
4	nr	nr	nr	nr	22.1/0.3/2.0	nr	nr	nr	na
5	nr	nr	nr	nr	na/na/5.0	nr	nr	nr	na
6	nr	nr	nr	nr	15.9/0.2/31.8	nr	nr	nr	y/n
7	3.4/7.9/41.2	3.5/5.2/39.6	3.2/1.4/30.9	nr	5.8/5.6/20.3	6.2/3.9/20.3	nr	na	y/n
8	3.3/16.8/42.2	3.8/3.9/36.5	2.3/7.4/43.5	nr	5.4/7.5/35.2	4.5/8.8/38.11	0.5/0.5/22.9	na	n/y
9	2.8/26.6/46.7	3.1/22.3/45.1	nr	nr	4.7/11.2/46.7	3.7/11.7/50.0	nr	na	y/n
10	3.9/8.0/34.8	2.3/12.0/50.0	na	nr	3.9/2.0/19.8	5.6/6.0/23.8	13.2/0.8/8.1	nr	y/na

B. Nerve conduction studies

	Sensory Nerves (DL/Amp/CV)[1]				Motor Nerves (DL/Amp/CV)				C/T[2]
	median	**ulnar**	**radial**	**sural**	**median**	**ulnar**	**peroneal**	**tibial**	
11	nr	nr	na	nr	15.5/1.0/nr	9.9/1.1/8.0	nr	15.3/1.0/nr	y/na
12	na	na	na	na	4.1/10.6/na	4.0/9.3/53	9.2/2.0/27	7.0/5.8/40	na a

[1] UE (D/P) = upper extremity (distal/proximal muscle strength on MRC);

[2] LE (D/P) = lower extremity (distal/proximal muscle strength on MRC);

[3] SF = sensory function;

[4] Trau = trauma history;

[5] CNS = central nervous system;

[6] F/U = rapidly progressive asymmetric weakness in follow up visit;

[7] Dec = decrease;

[8] intronic mutation;

[9] n/a = not available;

[10] c1184 – 1186, 3 base pair in-frame deletion of TTG (codon 395 – 396);

[11] All scores under this column were CMTES, but case 4 was a CMTPedS of 34;

[12] nl = normal;

* novel mutations; note that, in the case 12, copy number variation was excluded by a built-in protocol in the Next-Gen Sequencing and confirmed by a verification test. Thus, homozygous mutation of I41T in the case was validated.

[1] distal latency (ms) / amplitude (mV) / conduction velocity (m/s);

[2] Conduction block / temporal dispersion;

[3] non-responsive;

[4] not available